J Ther Eng, Vol. 11, No. 2, pp. 493−507, March, 2025

Journal of Thermal Engineering
Web page info: https://jten.yildiz.edu.tr
DOI: 10.14744/thermal.0000929

Research Article

Influence of curved trapezoidal winglet vortex generators on thermal-hydraulic performance in fin-and-tube heat exchangers

Alisan GONUL[1,*]

[1]*Department of Mechanical Engineering, Siirt University, Siirt, 56100, Türkiye*

ARTICLE INFO

Article history
Received: 30 December 2024
Revised: 16 February 2025
Accepted: 17 February 2025

Keywords:
Curved Trapezoidal Winglet Vortex Generators; Heat Transfer Enhancement; Response Surface Methodology

ABSTRACT

Fin-tube heat exchangers play a crucial role in various industrial and HVAC applications due to their high heat transfer efficiency. This study focuses on the numerical analysis of fin-tube heat exchangers integrated with curved trapezoidal winglet vortex generators. In the current work, the impact of three key factors on heat transfer and flow characteristics: inlet velocity (2–5 m/s), vortex generator position angle (45°–120°), and arc length (3.80–6.33 mm) is analyzed. To enhance the accuracy of output predictions, this research extends beyond conventional parametric studies by utilizing a structured design of experiments approach. The study determines the optimal configurations through Kriging response surface methodology analysis. Results indicate a potential 48.5% improvement in heat transfer and up to an 18.3% enhancement in thermo-hydraulic performance. Moreover, the study reveals that improper sizing and positioning of vortex generators may lead to a 5% decrease in thermo-hydraulic performance compared to the heat exchanger without vortex generators. This work aims to explore strategies for enhancing the thermal performance of fin-and-tube heat exchangers through novel vortex generator designs by considering their geometric dimensions and positioning.

Cite this article as: Gonul A. Influence of curved trapezoidal winglet vortex generators on thermal-hydraulic performance in fin-and-tube heat exchangers. J Ther Eng 2025;11(2):493−507.

INTRODUCTION

The fin-and-tube heat exchanger (FTHE) is widely used in sectors such as energy, automotive, and aerospace, owing to its compact structure and high heat transfer efficiency [1, 2]. Various strategies have been developed to enhance heat transfer performance while minimizing pressure drop in these systems. One such approach involves the use of vortex generators (VGs), which improve fluid mixing along heat exchange surfaces by inducing vortices in the flow. These VGs contribute to increased thermal convection and help mitigate boundary layer effects [3–5]. Additionally, the formation of turbulent flow leads to a noticeable improvement in the heat transfer coefficient.

Considering FTHEs, after the incoming flow impacts the tube, a boundary layer begins to develop along its surface and gradually thickens. Depending on the flow conditions, separation occurs at a certain point, leading to the formation of wake regions in the downstream area, which

***Corresponding author.**
*E-mail address: alisan.gonul@siirt.edu.tr

This paper was recommended for publication in revised form by Editor-in-Chief Ahmet Selim Dalkılıç

are characterized by low-velocity zones. To enhance thermal performance and reduce pressure losses, activating these wake regions using vortex generators is considered an effective strategy [6].

Researchers have investigated the impact of various vortex generator geometries including wing and winglet types [7]. On the other hand, wing-type VGs are classified as transverse vortex generators (TVG), whereas winglet-type VGs fall into the category of longitudinal vortex generators (LVG). Winglet-type vortex generators are known to generate more effective secondary vortices than wing-type VGs, resulting in superior overall performance. Their ability to enhance heat transfer while minimizing flow losses makes LVGs particularly advantageous for applications demanding high efficiency with reduced pressure drop [8]. Various LVG geometries have been developed, with the most common designs focusing on delta [9, 10], trapezoidal [11], and rectangular winglets [7, 10], on the performance of FTHE. According to these researches, vortex generators may impede fluid flow; nevertheless, this additional pressure loss typically does not negate the enhanced heat transfer. Leu et al. investigated the potential of block-shaped vortex generators to enhance FTHE performance and discovered that positioning vortex generators at a 45° angle can increase heat transfer by 25% in wake regions [12]. Samadifar and Toghraie examined six distinct models of vortex generators and determined that rectangular vortex generators were 7% more effective at heat transfer than the other variants. They also reported that 45° is the optimal angle for implementation [13]. Biswas et al. highlighted that delta winglet vortex generators significantly enhance the heat transfer coefficient by disrupting the thermal boundary layer on FTHE surfaces; however, this improvement comes at the cost of increased pressure drop [7]. Chien-Nan Lin et al. demonstrated that the utilization of oval tubes and angled block vortex generators can reduce pressure loss by up to 35% and enhance heat transfer by as much as 16% [14]. Xie and Lee demonstrated that curved rectangular vortex generators can enhance the thermal performance in FTHE by 30–50% and developed new correlations to assist designers in optimizing their designs [15]. Oh and Kim investigated curved VG applications in a staggered tube arrangement, examining the effects of different positioning angles. Their study analyzed both rectangular and delta-type curved VGs, highlighting that VG positioning plays a crucial role in enhancing heat transfer. It was reported that the use of curved rectangular vortex generators (VGs) in FTHEs resulted in up to a 40% improvement in thermal performance [6]. Similarly, Lin et al. conducted studies on delta-curved vortex generators, showing that employing curved delta winglets enhanced heat transfer by approximately 28% [16]. Sharma et al. investigated the effect of curved trapezoidal VGs in FTHEs using the Response Surface Methodology (RSM) and Artificial Neural Networks (ANN). They considered tube diameters ranging from 8 to 11 mm, VG positioning angles between 30° and 75°, and VG-defining dimensions as variables. The findings demonstrated that both RSM and ANN are highly effective computational methods. Notably, improvements of up to 117% were achieved compared to the reference case [17]. Saleh et al. experimentally analyzed the heat transfer effects of both flat and curved trapezoidal VGs in FTHEs. Their study investigated the influence of VG dimensions, attack angles (10°–90°), and Reynolds numbers (500–2500). In the reference case, a large wake region was observed. The results showed that while larger positioning angles increased pressure drop, they also significantly enhanced heat transfer performance [11]. Similarly, Sarangi et al. employed a numerical approach to investigate the effects of attack angle (30°–75°), Reynolds number (300–600), and VG height on curved trapezoidal vortex generators. The results indicated that optimal performance was achieved at an attack angle of approximately 70° [18]. Among various VG geometries, rectangular winglet, trapezoidal winglet, and delta winglet VGs are frequently applied in FTHEs, with trapezoidal winglets being reported as the most effective [19]. The incorporation of vortex generators in FTHE systems is a significant improvement that enhances the efficiency of compact systems and promotes energy conservation as seen in the previous works. Future computational and empirical investigations are anticipated to identify optimal methods for enhancing the efficacy of these systems. It is asserted that the positioning and design of vortex generators significantly enhance thermal performance.

This work emphasizes the substantial influence of vortex generators on improving FTHE performance, while also highlighting the necessity of identifying the optimal designs for each specific application. In particular, compared to research on delta and rectangular curved vortex generators, studies on curved trapezoidal vortex generators are notably scarce in the literature. This study aims to explore the optimal performance of novel curved trapezoidal vortex generator designs, examining their positioning and dimensions relative to the tube under various flow conditions. The analysis considers arc angles ranging from 30° to 50° and position angles between 45° and 120°, with inlet velocities spanning from 2 to 5 m/s. To achieve this, the Kriging Response Surface Method is employed to process data generated using Central Composite Design and Box-Behnken design of experiment methodologies. This comprehensive approach offers valuable insights into achieving superior thermal performance with curved trapezoidal vortex generators. Simultaneously, it underlines the consequences of thermal-fluid performance decrease that may arise from inappropriate sizing and positioning.

NUMERICAL MODELING

ANSYS Fluent 21.1 software is employed in this study to simulate the thermal-flow behavior within a FTHE. In this section, the dimensions of the FTHE and VG used in the study, the details of the applied mesh structures, the

boundary conditions, and the relevant equations are presented sequentially.

Geometric Structure and Dimensions

The dimensions and arrangement of the fin and tube heat exchanger and vortex generators used in the study are illustrated in Figure 1. The region represented by dashed lines corresponds to the area analyzed in the CFD simulations. The total length of the heat exchanger is set to 167.5 mm, with a tube-to-tube traverse distance of 25 mm and a channel height of 4 mm. The tube diameter is 9.5 mm, while the longitudinal spacing between the tubes is 29.50 mm. The vortex generator has a distance of 2.5 mm from the tube and a thickness of 0.25 mm. In the literature, it has been observed that vortex generators exhibit the most effective heat transfer performance when their length is half the channel length. Based on this, a height of 2 mm is selected [20, 21]. Additional dimensional details can be found in Figure 1. The position angle (α) and the angles defining the curved vortex generator arc length (β) are also depicted in the figure. Examples of arc lengths corresponding to different β angles are provided within the figure. In the literature, the positioning angle is considered a crucial parameter in determining the heat transfer performance characteristics of a heat exchanger equipped with CVGs. It has been specifically noted that both low and high positioning angles contribute to heat transfer enhancement. When $\alpha < 90°$, effective mixing occurs, leading to increased heat transfer around the junction on the convex side of the CVGs. Conversely, when $\alpha > 90°$, the flow directed by the concave side of the CVGs improves weak heat transfer regions and reduces the wake size behind the tube [6]. In this study, a wide range of angles from 45° to 120° is considered to provide a detailed analysis of the effect of the positioning angle. Moreover, research indicates that as the size of the winglet increases, a greater portion of the primary flow is redirected toward the thermal isolation zone. This redirection enhances thermal mixing while minimizing the formation of large vortices in that region [17]. Therefore, in this study, arc lengths of different sizes are also analyzed. The β angle, which determines the arc length, ranges from 30° to 50°.

Computational Domain and Boundary Conditions

The boundary conditions and mesh details used in the computational domain for the CFD analysis are illustrated in Figure 2(a). The inlet boundary is specified as a velocity inlet, with velocity values ranging from 2 to 5 m/s, selected based on operational requirements. These velocity ranges are frequently utilized in practical applications and align with findings from previous studies [15, 22, 23]. The top and bottom walls of both the inlet and outlet domains are assigned a slip condition with a pressure of 0 Pa, while a constant temperature boundary condition is imposed on the top and bottom surfaces of the test region. Likewise, the outer surfaces of the tubes are subjected to a constant temperature boundary condition. Since aluminum, known for its high thermal conductivity, is used for the fins, this boundary condition is commonly adopted in literature [24]. Due to both the surface temperatures in practical applications and the assumption of constant surface temperature, radiation effects have been neglected. Symmetry boundary

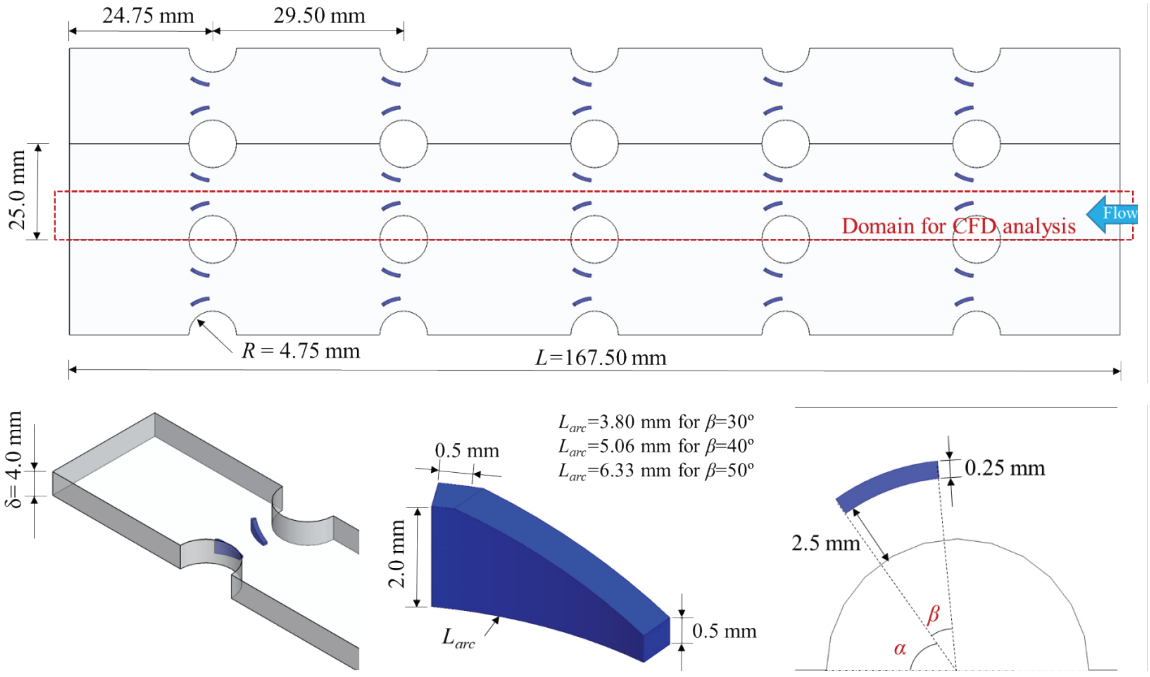

Figure 1. Dimensional and placement details of the novel CVG and FTHE.

conditions are defined on the side surfaces of the inlet and outlet domains, as well as the test domain. In the study, temperature, pressure, and velocity contours are obtained from various planes to interpret the physics of the flow. The relevant adjustments are provided in Figure 2. The origin of the coordinate system (x= 0, y= 0, z= 0) is set at the bottom-left corner of the test domain inlet. Plane 1 is defined at y-direction 1 mm. Planes 2, 3, 4, and 5 are defined along the x-direction at 62.5 mm, 67.5 mm, 72.5 mm, and 77.5 mm, respectively.

Aluminum (Al) is preferred due to its high thermal conductivity, lower weight compared to alternative materials such as copper, high corrosion resistance, cost-effectiveness, and recyclability [25, 26]. Therefore, aluminum has been utilized in fins and vortex generators. Considering the application requirements, air has been selected as the coolant. The properties of air and aluminum are presented in Table 1 below.

A hexahedral mesh is applied to the upstream and downstream regions, while a tetrahedral mesh is used for the test zone. To more accurately capture boundary layer interactions, 10 inflation layers are generated. Detailed information regarding the mesh structure is provided in Figure 2(b).

Table 1. Thermophysical properties of Al [27] and air [24]

Properties	Al	Air
ρ (kg.m^{-3})	2719	1.205
k (W.m^{-2}.K^{-1})	202.4	0.0259
C_p (J.kg^{-1}.K^{-1})	871	1005
μ (Pa.s)	---	1.81e-05

Governing Equations and Turbulence Model

In FTHEs with vortex generators, heat transfer is influenced by the conjugate heat transfer mechanism. The governing equations for heat conduction in the solid region and heat convection between the solid and fluid regions are solved simultaneously. When these transport

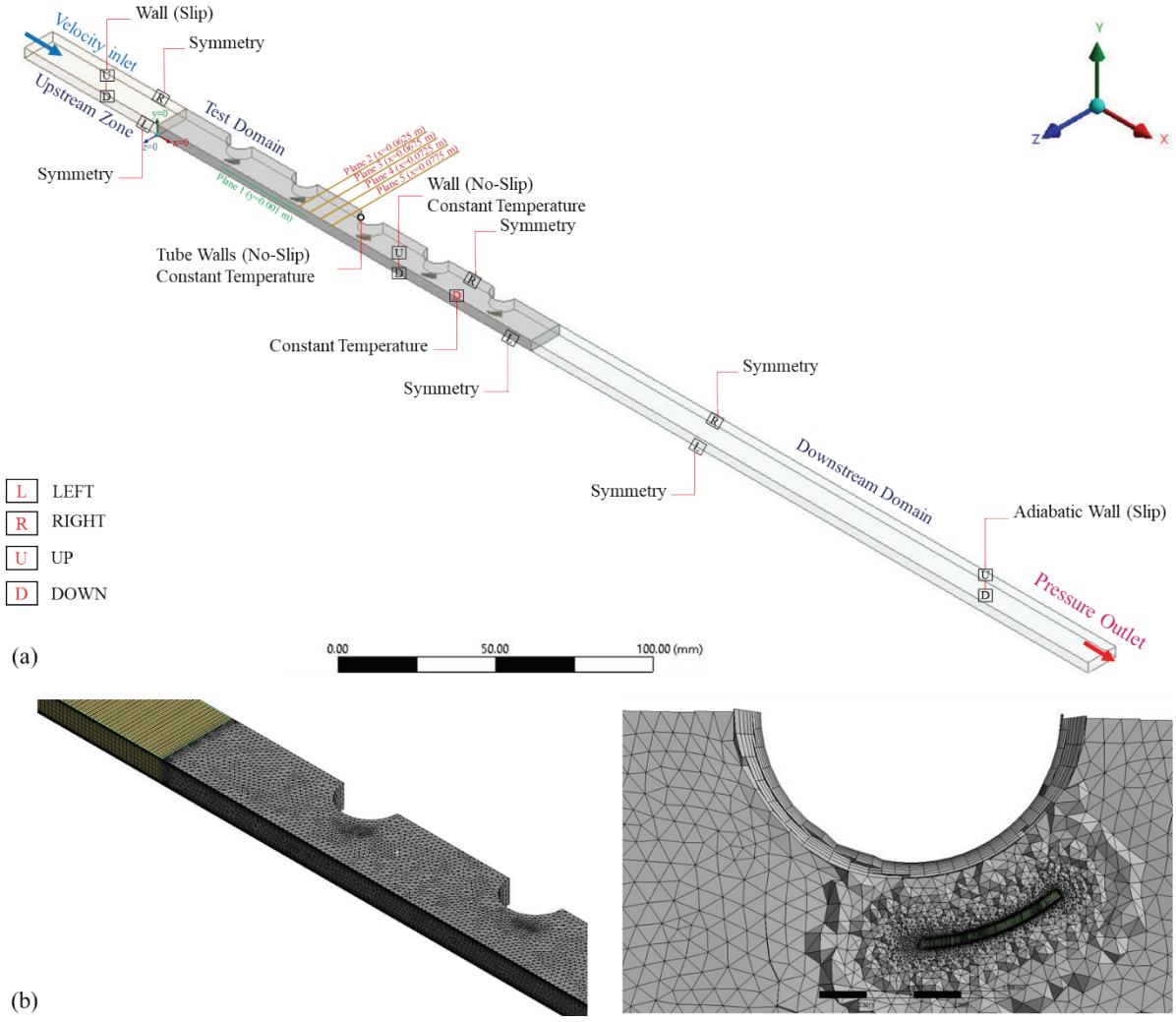

Figure 2. (a) Boundary conditions and (b) Mesh detail of computational domain for related FTHE with CVGs.

and governing equations are time-averaged, the Reynolds-averaged Navier-Stokes (RANS) equations are obtained. The density of both the solid and fluid domains is considered constant, and the impact of radiation is neglected. Under steady-state conditions, the continuity, momentum, and energy equations for both fluid and solid regions are formulated as follows [28]:

The continuity equation,

$$\frac{\partial u_i}{\partial x_j} = 0 \tag{1}$$

The momentum equation,

$$\rho u_j \frac{\partial u_i}{\partial x_j} = -\frac{\partial P}{\partial x_i} + \frac{\partial}{\partial x_j}\left((\mu+\mu_t)\frac{\partial u_i}{\partial x_j}\right) \tag{2}$$

The fluid domain's energy equation,

$$\rho c_p \left(u_i \frac{\partial T}{\partial x_j}\right) = \frac{\partial}{\partial x_j}\left((k+k_t)\frac{\partial T}{\partial x_j}\right) \tag{3}$$

The solid domain's energy equation,

$$k_s \frac{\partial^2 T}{\partial x_j^2} = 0 \tag{4}$$

x_j represents the x, y, and z coordinates in the Cartesian coordinate system for j = 1, 2, 3, respectively. Below are several parameters provided to assess the thermal and flow performances in FTHE with VGs. The Shear Stress Transport (SST)-kω model is utilized in the analysis by considering the turbulence intensity in the flow. Numerical investigations of FTHE applications related to this model are frequently conducted in the literature [11, 17, 18]. The governing equations are discretized using a second-order upwind scheme, ensuring higher accuracy in spatial resolution. The Coupled pressure-velocity coupling method is applied to enhance numerical stability and accelerate convergence. The residuals for the continuity, momentum, and turbulence-related equations are monitored and set to convergence criteria of 10^{-4} for continuity and 10^{-8} for energy, ensuring solution stability and reliability.

Performance Evaluation Parameters

In this section, the definitions of the formulas used in the analysis of the thermal-flow characteristics considered in the study are provided.

The Reynolds numbers (Re) are calculated as follows [22]:

$$\mathrm{Re} = \frac{\rho V_m D_h}{\mu} \tag{5}$$

Here, V_m represents the average velocity at the narrowest cross-section, ρ denotes the fluid density, μ indicates the fluid viscosity, and D_h refers to the hydraulic diameter and is calculated using the following equation:

$$D_h = \frac{4V_t}{A_t} \tag{6}$$

where, V_t represents the total volume of heat transfer, A_t represents the total area of heat transfer.

The dimensionless average Nusselt number (Nu), which serves as a crucial indicator of heat transfer performance, is defined as follows:

$$\mathrm{Nu} = \frac{h_c D_h}{k_f} \tag{7}$$

where h_c is the heat convection coefficient, calculated using the formula:

$$h_c = \frac{\dot{Q}}{A_h \Delta T_m} \tag{8}$$

here $\dot{Q}$, ΔT_{m}, and A_h denote the heat transfer rate, the logarithmic mean temperature difference (LMTD), and the total heat transfer surface area, respectively. The LMTD is expressed as:

$$\Delta T_m = \frac{T_o - T_i}{ln\left(\frac{T_w - T_i}{T_w - T_o}\right)} \tag{9}$$

Here, T_w represents the tube and fin wall temperature, while T_o and T_i denote the outlet and inlet temperatures, respectively. The apparent Darcy friction factor, f is defined as:

$$f = \frac{2\Delta P D_h}{\rho V_m^2 L} \tag{10}$$

To better represent the thermal-hydraulic performance, PEC, which correlates heat transfer and pressure characteristics with and without vortex generators (VGs), is introduced:

$$PEC = \frac{\mathrm{Nu}/\mathrm{Nu}_0}{(f/f_0)^{1/3}} \tag{11}$$

A pressure-based solver is utilized for the simulations, with the coupled algorithm chosen to handle velocity-pressure coupling. Spatial discretization of the governing equations is carried out using a second-order upwind scheme. To enhance accuracy and address potential mesh imperfections, particularly those related to orthogonality, the least squares gradient method is employed. The residuals of the

continuity, momentum, and energy equations are verified to converge to values below 10^{-4}, 10^{-7}, and 10^{-8}, respectively.

Validation Studies

To ensure the accuracy and reliability of numerical models, it is crucial to validate them against experimentally established studies widely accepted in the literature and to perform grid independence analyses. In this context, a comparison was made with the well-known correlations for Nu and *f* proposed by Zhukauskas and Ulinskas [29]. These correlations are frequently used for the numerical validation of fin-and-tube heat exchangers [30, 31]. A model has been developed to compute heat transfer and pressure drop in tube bundles using the SST-kω turbulence model, considering the tube diameters and spacing employed in this study. Heat transfer calculations have been evaluated based on the Nu, and the corresponding comparison correlation is provided in Eq.12 [29].

$$\mathrm{Nu} = 0.27F\mathrm{Re}_D^{0.63}\mathrm{Pr}^{0.4}(\mathrm{Pr}/\mathrm{Pr}_s)^{0.25} \tag{12}$$

In the calculation of the Re, the tube diameter is taken as the characteristic length, while the velocity is determined based on the average velocity at the narrowest cross-section within the tube bundle. Note that all properties, except for Pr_s, should be evaluated at the arithmetic mean temperature of the fluid, whereas Pr_s must be calculated based on the tube surface temperature. The correction factor (F) is 0.93 for a five-row tube bundle [32].

The friction factor in tube bundles is calculated using the following formula, where N_L represents the number of consecutive tube rows, and χ is the correction factor used in the friction factor calculation. The values of f_{TB} and χ are determined using graphs developed by Zukauskas and Ulinskas, which account for different Reynolds numbers and arrangement conditions [29].

$$f_{TB} = \frac{2\Delta P}{N_L \chi \rho V_m^2} \tag{13}$$

Figure 3(a) presents a comparison between the numerical results obtained for varying Re and the correlation proposed by Zukauskas and Ulinskas [29]. It is observed that both approaches exhibit a similar trend, with a maximum deviation of approximately 9%. Figure 3(b) illustrates the effect of varying Re on the f_{TB}. According to the graphs developed by Zukauskas and Ulinskas [29], for in-line tube bundles, the friction factor f_{TB} remains approximately constant at 0.16 for the considered range of Re and S_L/D values. The numerical results closely align with this value, although a slight decrease is observed at higher Re values. In the end, the numerical and experimental findings show a high level of consistency. This indicates that the methods employed in this investigation are appropriate for projecting the performance of heat exchangers.

Mesh Independence Analysis

Mesh independence analyses are conducted by examining the variation in Nu and *f* under the conditions of α = 90°, V_i = 5 m/s, and β=50° for mesh sizes of 0.4, 1.1, 2.7, and 6.8 million elements. The results, presented in Table 2,

Table 2. Mesh independence study of FTHE with curved trapezoidal VGs

No	Number of mesh elements	*Nu*	*f*
1	436287	21.40	0.139
2	1125640	20.90	0.128
3	2733319	20.70	0.121
4	6845368	20.68	0.120

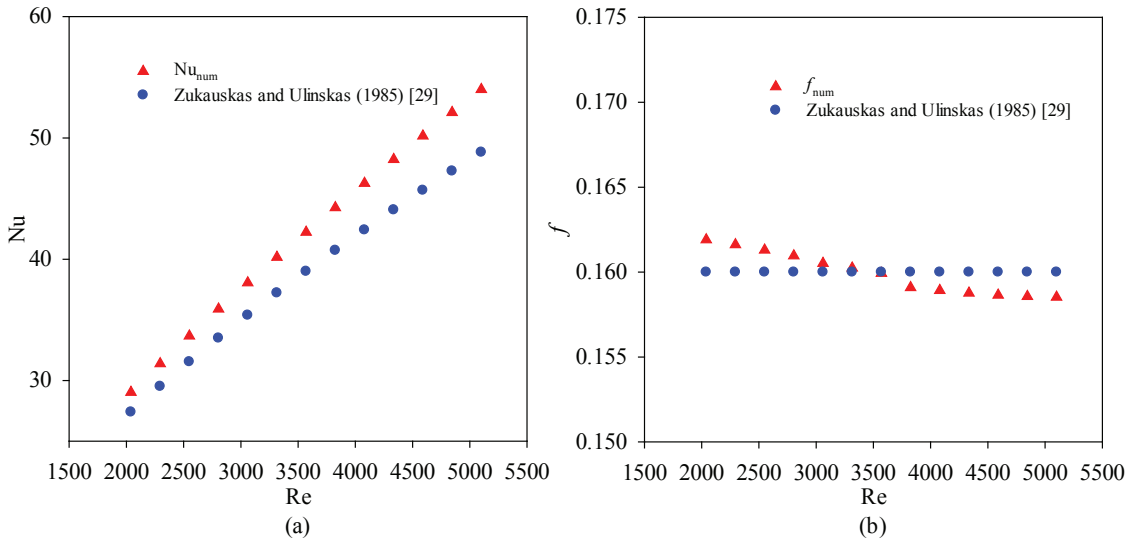

Figure 3. Validation Comparisons: Variation of (a) Nu and (b) f_{TB} with Re.

indicate no significant differences between the 1.1 million and 6.8 million element meshes. However, for enhanced precision in the Design of Experiments (DOE) and parametric studies, the mesh structure with 2.7 million elements was selected for further simulations.

RESULTS AND DISCUSSION

The results regarding the effects of heat transfer and pressure drop due to the application of the novel CVG in FTHEs are presented in this section. The observed variations are analyzed and interpreted using velocity, temperature, and pressure contours obtained from various planes in the solution domain.

Parametric Studies on Thermal-Flow Characteristics

Figure 4 demonstrates the effects of the position angles of curved trapezoidal vortex generators (VGs) on heat transfer and pressure drop in the flow direction. The corresponding data are presented for an arc angle of 40° and a Re of 3006.

Figure 4(a) shows the variation of Nu with position angle, revealing that Nu decreases within the range of 45° to 60°. Beyond 60°, heat transfer improves significantly, reaching a maximum between 90-100°. After this point, heat transfer rapidly decreases, reflecting the dependency of flow resistance on the position angle. Similarly, Figure 4(b) indicates that the pressure drop exhibits a trend comparable to that of heat transfer enhancement. However, it is observed that the change in pressure drop within the range of 45° to 60° is relatively minimal. In Figure 4(c), it is evident that the application of VGs consistently improves heat transfer compared to the case without VGs. However, at both low and high position angles, the enhancement in heat transfer is relatively limited. This dimensionless representation reflects the relative increase in heat transfer rate compared to the reference case and demonstrates that maximum improvement occurs at an optimum position angle. The observed improvement reaches up to 48.5% at moderate position angles. It is observed that for angle values between 50°-65° and beyond 115°, the Nu values give close values compared to the baseline case. This indicates that while VGs are widely recognized as an effective method to

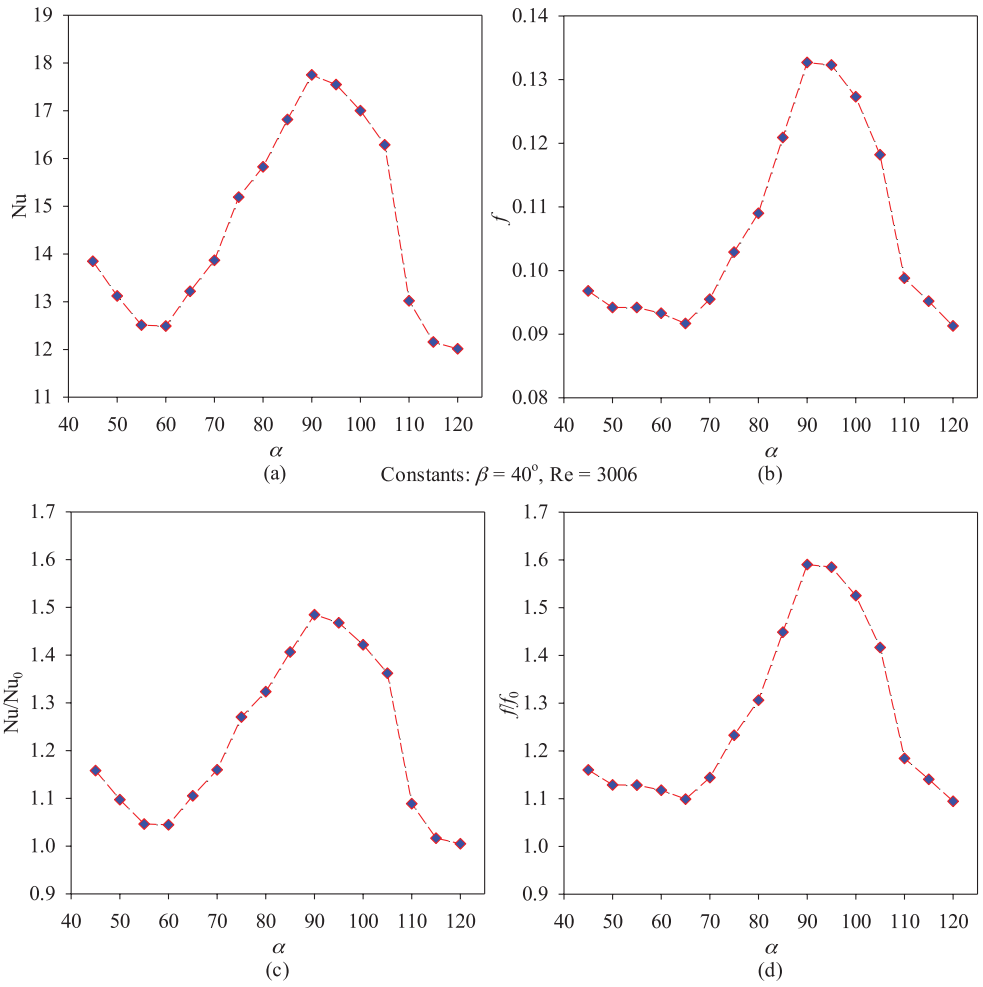

Figure 4. Variation of (a) Nu, (b) f, (c) Nu/Nu_0, and (d) f/f_0 with changes in the position angle of the vortex generator (α).

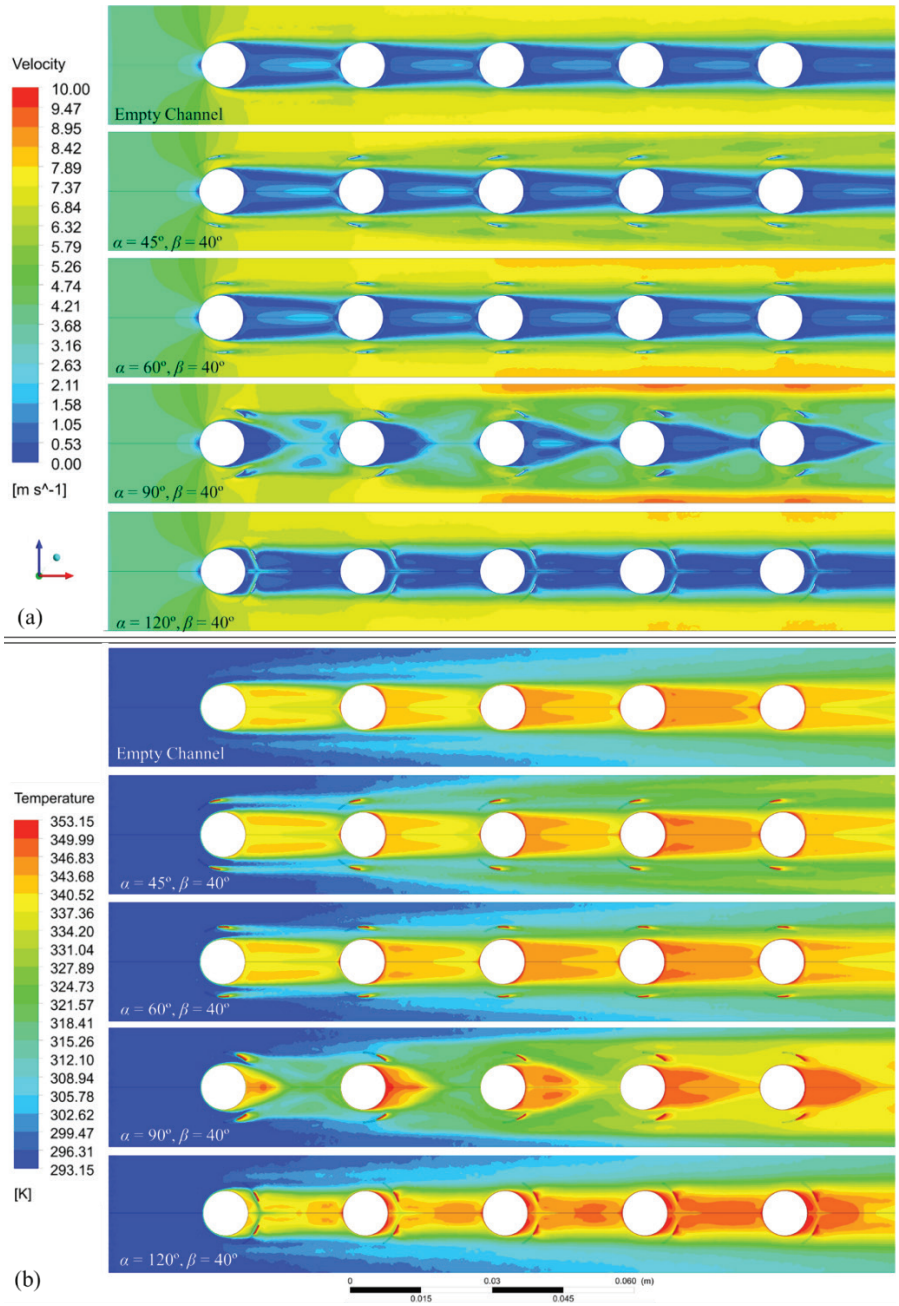

Figure 5. Distributions on Plane 1 for different position angles: (a) Velocity contour distribution, (b) Temperature contour distributions.

enhance heat transfer, improper sizing or positioning can lead to a decrease in system performance. However, as is well known, the addition of VGs increases the surface area in FTHEs. When this increase is accounted for in the Nu calculations, it should be noted that the normalized Nu ratios exceed at least 10%. Furthermore, when the surface area increase is incorporated into the Nu improvement, a thermal enhancement of up to 54%. Figure 4(d) exemplifies the variation in the friction factor compared to the reference case. The maximum friction factor at specific position angles can be as high as 64% above the baseline value. At both low and high position angles, while the thermal enhancement is minimal, the friction factor increases by more than 10%. Specifically, it is observed that thermal-hydraulic performance deteriorates by up to 5% compared to an FTHE without VGs at a position angle of 120°. Overall, the analysis across all figures suggests that the optimum position angle range is between 80° and 100°, where both heat transfer and the friction factor reach their respective maxima. To interpret the relevant results, velocity, temperature, and pressure contours for various cases are presented in Figures 5 and 6.

Figure 5(a) illustrates the distribution of vortex generators (VGs) placed on Plane 1 at position angles of 45°, 60°, 90°, and 120°, in addition to the empty (without VG) case. In this study, the beta angle was maintained constant at 40°. As observed in the figure, in the absence of VGs, the wake region formed behind the first tube significantly influences the flow over the subsequent tube rows in the array. The figure clearly demonstrates the occurrence of boundary layer separation and the resultant flow instabilities in the rear regions of the tubes. The presence of low-velocity flow regions within the wake interacts with the boundary layers of the subsequent tubes, thereby reducing the overall heat transfer along the tube bank. Similarly, in the configurations with position angles of 45° and 60°, no significant mechanism is observed to disrupt the structure of the low-velocity flow within the wake region. However, a partial increase in velocity is noted behind the VGs in these cases. Conversely, at a position angle of 90°, an analysis of the velocity distributions reveals an increase in turbulence levels and a more effective redirection of the flow, leading to a substantial reduction in the wake region's length. Under these conditions, the adverse thermal effects of the successive tube rows are mitigated, resulting in an enhancement of heat transfer. On the other hand, at a position angle of 120°, although the VGs partially redirect the flow behind the tubes, they are predominantly positioned within the low-velocity region. Consequently, the improvement in heat transfer remains limited. Song et al. investigated concave, convex, and flat vortex generators (VGs) in the flow direction. It has been reported that CVGs induce a secondary flow that enhances the heat transfer performance of the fin. While concave placement improves heat transfer at specific angles, when the α becomes too large, CVGs remain within the wake region of the tube, resulting in minimal effects on the system compared to conventional VGs [33]. In this study, VGs are convex up to 90° and concave beyond 90°, leading to a thermal behavior consistent with findings in the literature. Moreover, when the positioning angle exceeds 90°, the redirection of flow towards the wake region is reported to enhance heat transfer [6]. Figure 5(b) presents the corresponding temperature distributions for the scenarios illustrated in Figure 5(a). As anticipated, an increase in temperature is evident in the low-velocity regions. These regions exhibit considerable variations and high gradients in temperature distribution. Although the configurations with the empty channel, as well as those with 45° and 60° position angles, exhibit somewhat more homogeneous temperature gradients, they generally reflect similar distributions to the empty case. In the case of the 90° position angle, the improved velocity distribution effectively narrows and shortens the wake region, leading to a reduction in high-temperature regions and the formation of more uniform temperature gradients. This contributes to a more homogeneous thermal distribution across the section and minimizes hot spot formation, resulting in enhanced thermal performance of the system. Conversely, for the 120°

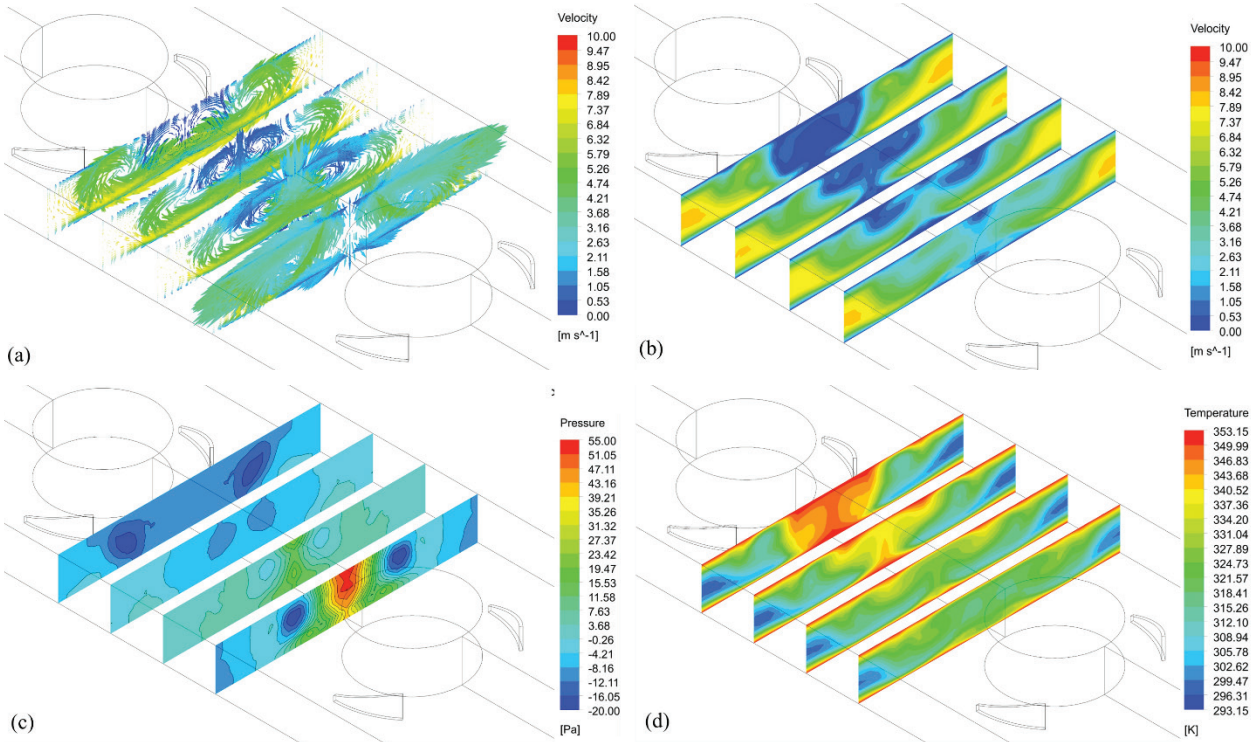

Figure 6. Distributions for α=90° and β=40° (a) Velocity vectors, (b) Velocity contours, (c) Pressure contours, (d) Temperature contours.

position angle, the placement of the VGs within the wake region results in a lack of temperature homogeneity, which, in parallel, does not contribute significantly to thermal performance improvement. The findings suggest that, within the examined range of position angles, the effectiveness of VG applications is limited at both low and high angles. However, particularly at the 90° position angle, substantial improvements in thermal performance are achieved. These results underscore the strategic importance of VG placement in optimizing thermo-fluid performance.

Figure 6 presents the velocity, pressure, and temperature distribution results across four different planes located between the 2nd and 3rd tubes in the flow direction at a 90° position angle. Examination of the velocity vectors and contours in Figures 6(a) and 6(b) reveals the formation of tip vortices originating from the long edges of the vortex generators (VGs). Depending on the positioning of the VGs, these vortices generate swirling motions that rotate both clockwise and counterclockwise. In addition to enhancing turbulence and improving mixing, they also help prevent the premature separation of the boundary layer on the tube surfaces. In general, it is observed that the flow is directed along the channel with higher velocity gradients due to the influence of the VGs. Nevertheless, although low-velocity regions are not completely eliminated along the channel, the flow is effectively guided by the high-velocity gradients generated by the VGs. The observation that the flow velocity is higher near the edges and lower in the central regions highlights the importance of optimizing VG placement. The effect of VGs results in a reduced spread of the wake region and a redistribution of velocity between the tubes. Analysis of the variations between successive planes indicates that the influence of VGs significantly disrupts the velocity and thermal boundary layers in the lower regions, leading to the effective mixing of velocity distributions across the cross-sections. This effect reduces the interaction between successive tubes, allowing each tube to function more independently. The independent operation induced by the VGs results in high-pressure regions forming on the front surfaces of the tubes and low-pressure regions on the rear surfaces. As shown in Figure 6(c), the high-pressure regions formed on the front surfaces of the tubes in successive rows contribute to a more efficient and homogeneous velocity distribution within the flow. Moreover, the fact that

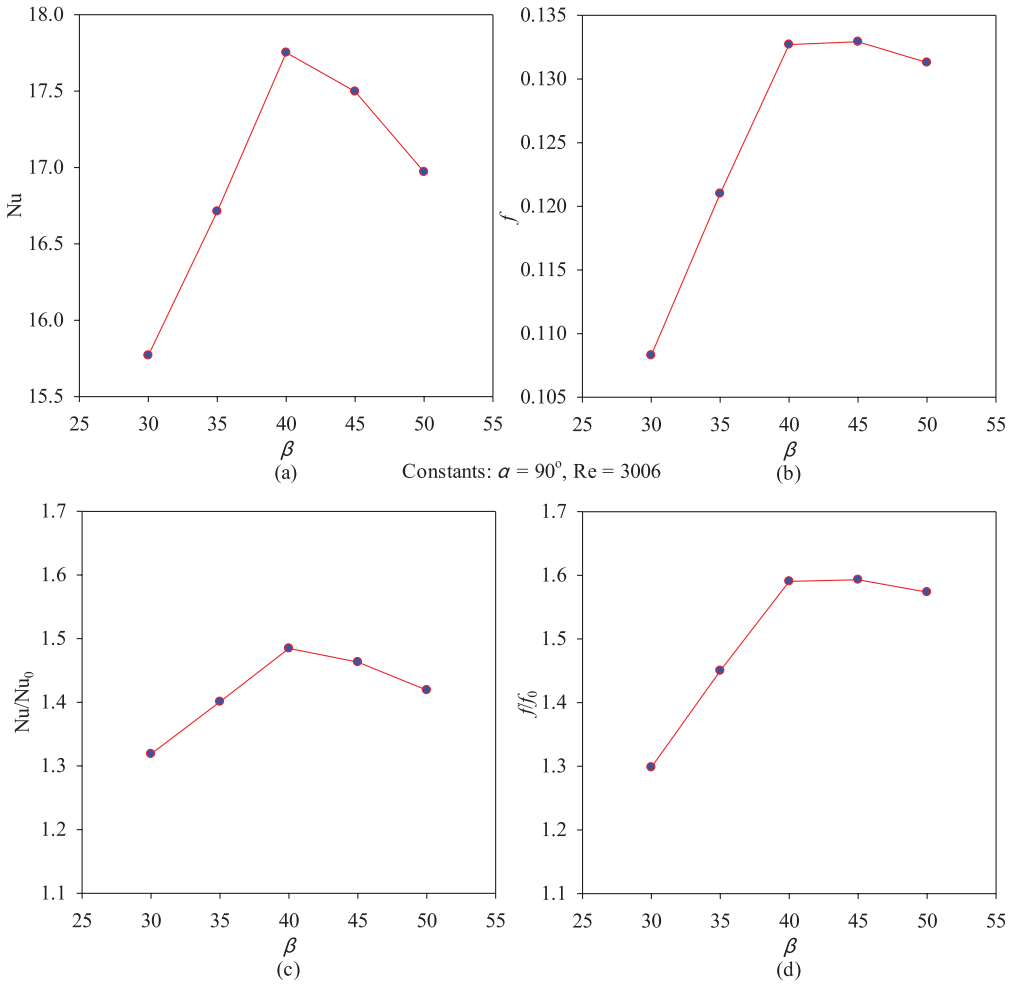

Figure 7. Variation of (a) Nu, (b) f, (c) Nu/Nu_0, and (d) f/f_0 with changes in the arc angle of the curved vortex generator.

low-pressure regions are not excessively extended indicates that the VGs have been effectively positioned, minimizing flow separation. Consequently, it can be inferred that the pressure drop has been partially reduced. The findings obtained demonstrate that VGs effectively disrupt thermal boundary layers, leading to a more homogeneous temperature distribution across the cross-section. In particular, within the flow between the tubes, high-temperature regions (represented by red and yellow tones) are observed to be more widely distributed, with a reduction in localized overheating spots. The sequential plane visualizations presented in Figure 6 clearly indicate that the velocity and

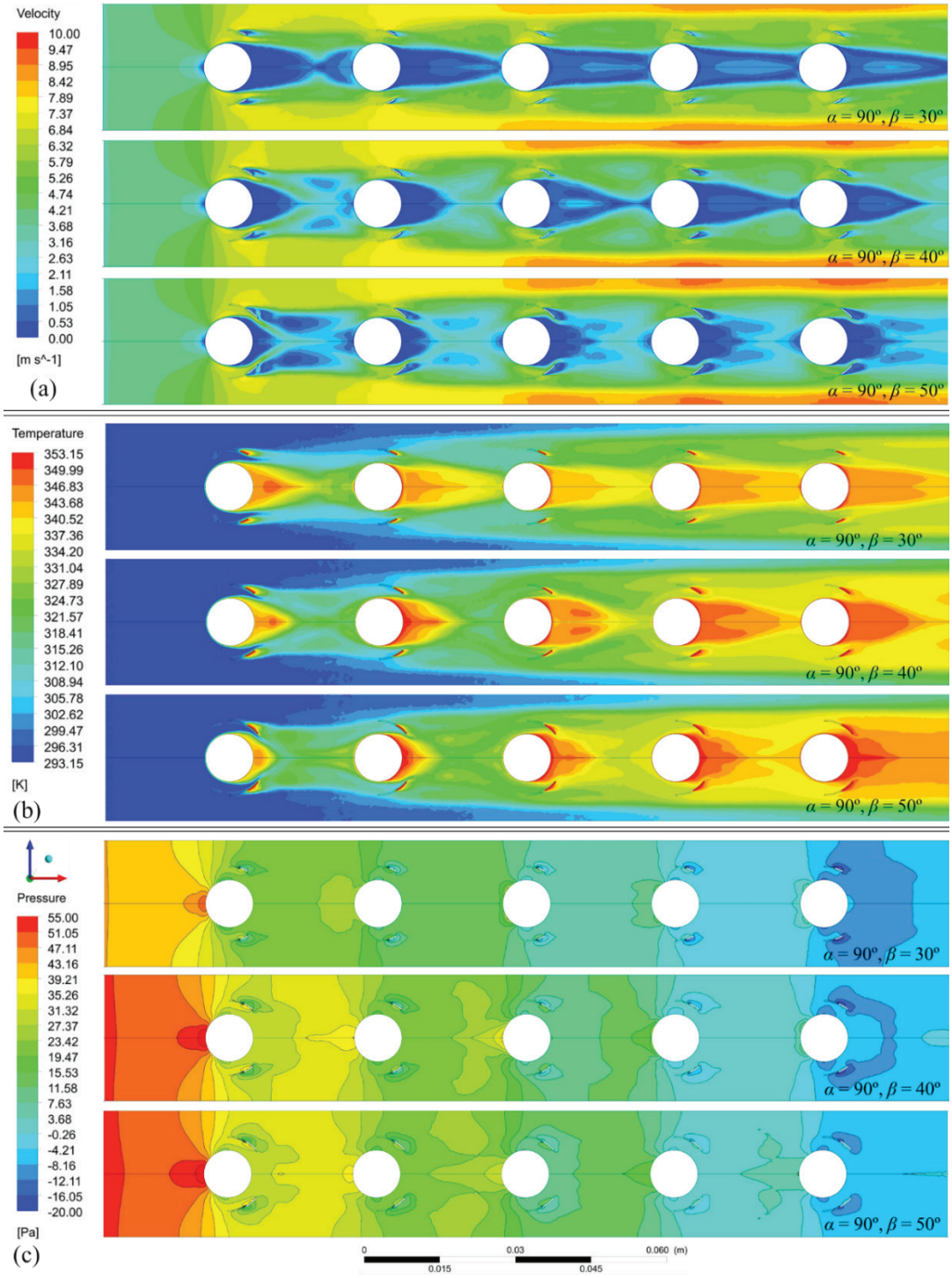

Figure 8. Distribution of (a) velocity contour, (b) temperature contour, and (c) pressure contour on Plane 1 for different arc lengths.

temperature distributions have been optimized, contributing to an overall enhancement of the system's thermal performance.

Figure 7 illustrates the effects of the arc angle or arc length in curved vortex generator applications. The figures are generated for a position angle of 90° and Re of 3006. Figure 7(a) illustrates the variation of Nu with respect to the arc angle. It is observed that as the arc angle increases from 30° to 40°, the Nu value consistently rises, indicating an improvement in heat transfer by approximately 13%. However, beyond 40°, a decline in heat transfer is noted. This underscores the importance of selecting an optimal arc length to achieve significant enhancement in heat transfer performance. Figure 7(b) presents the variation of the friction factor with the arc angle. Although the behavior is relatively similar to that of heat transfer, it is observed that the f value remains relatively unchanged between 40° and 50°. When the arc angle increases from 30° to 40°, the friction factor rises by approximately 23%, emphasizing the trade-off between enhanced heat transfer and increased flow resistance. The normalized values of heat transfer and pressure drop, compared to a system without vortex generators, are depicted in Figures 7(c) and 7(d). The normalized Nusselt number (Nu/Nu_0) shows an improvement ranging from 30% to 48.5% as the arc length increases. Conversely, the normalized friction factor (f/f_0) varies between 30% and 57%, depending on the arc angle performance parameters. Figure 8 presents velocity, temperature, and pressure contours for different cases to facilitate the interpretation of the relevant results.

The effects of varying VG arc lengths at different beta angles on flow characteristics are presented in Figure 8 for a α of 90° and a Re of 3006. When examining the velocity distributions corresponding to different arc lengths in Figure 8(a), it is observed that increasing the arc length significantly enhances flow separations around the pipe. For shorter arc lengths, low-velocity regions remain limited, whereas in high-velocity regions, the wake zones behind the VGs expand considerably. This indicates that shorter arc lengths have a limited effect on flow guidance and increase the interaction between the pipes. On the other hand, longer arc lengths generate broader wake regions in the downstream areas of the VGs, resulting in greater flow disruption. Longer VGs may increase turbulence, potentially affecting the overall efficiency of the system. Figure 8(b) presents the temperature distribution on Plane 1. In general, a temperature decrease is observed along the flow direction. VGs with shorter arc lengths create extended thermal regions behind the pipe, enhancing thermal mixing, whereas longer arc lengths cause the hot regions to be confined to a narrower area. This suggests that longer VG arc lengths improve heat management and reduce temperature gradients. Figure 8(c) displays the pressure distributions for different VG arc lengths. As the VG arc length increases, high-pressure regions in front of the tube become more pronounced. This indicates that longer VGs create greater resistance to the incoming flow. At the same time, low-pressure regions behind the tube expand, leading to a larger overall pressure drop across the system. Consequently, this results in an increase in drag forces and energy losses. In conclusion, selecting an appropriate VG arc length is critical for optimizing flow characteristics. While shorter arc lengths have a limited effect on flow control and help reduce energy losses, longer arc lengths enhance flow separation and mixing but lead to higher drag forces and pressure drops. Therefore, in engineering applications, a balanced approach should be adopted to ensure an optimal trade-off between flow control, heat management, and energy efficiency.

Response Surface Methodology Studies

Response Surface Methodology (RSM) is a statistical and mathematical approach used to model and optimize the effects of one or more independent variables on a target (dependent) variable. This methodology, particularly when combined with a specific Design of Experiments (DOE) approach, enables the modeling of relationships between dependent and independent variables. In recent years, the design of experiments (DOE) and response surface methods (RSM) have been widely applied to experimental and numerical studies while facilitating the interpretation of results. These approaches significantly reduce the number of experiments required, offering a more efficient alternative to traditional experimental techniques [34]. This approach was initially developed by Box and Wilson [35].

In this study, the experiments were conducted using the Box-Behknen and Central Composite Design (CCD) [36] as the DOE approach and the Kriging method [9] as the RSM, implemented via the ANSYS DesignXplorer software [37]. The Kriging RSM extends the classical RSM models, which are based on linear or second-order polynomials, offering a more flexible and robust approach. This method overcomes the limitations of traditional RSM, particularly for nonlinear and complex processes [9].

The Kriging model fundamentally represents a function as follows:

$$y(x) = \mu + Z(x) \tag{14}$$

Here, μ represents the general trend (deterministic component) and $Z(x)$ represents the stochastic process; a random component with a mean of zero and a specific covariance structure. The covariance structure determines the accuracy of the predictions based on the spatial proximity of the data points. As a result of the study, the Kriging RSM demonstrated its effectiveness for the curved trapezoidal FTHE, yielding an R^2 value close to 1 and an RMSE near zero. This confirms that Kriging RSM is a highly effective approach for this application.

Figure 9 presents the variation in PEC values obtained through the Kriging RSM based on the interactions of the considered parameters in a three-dimensional

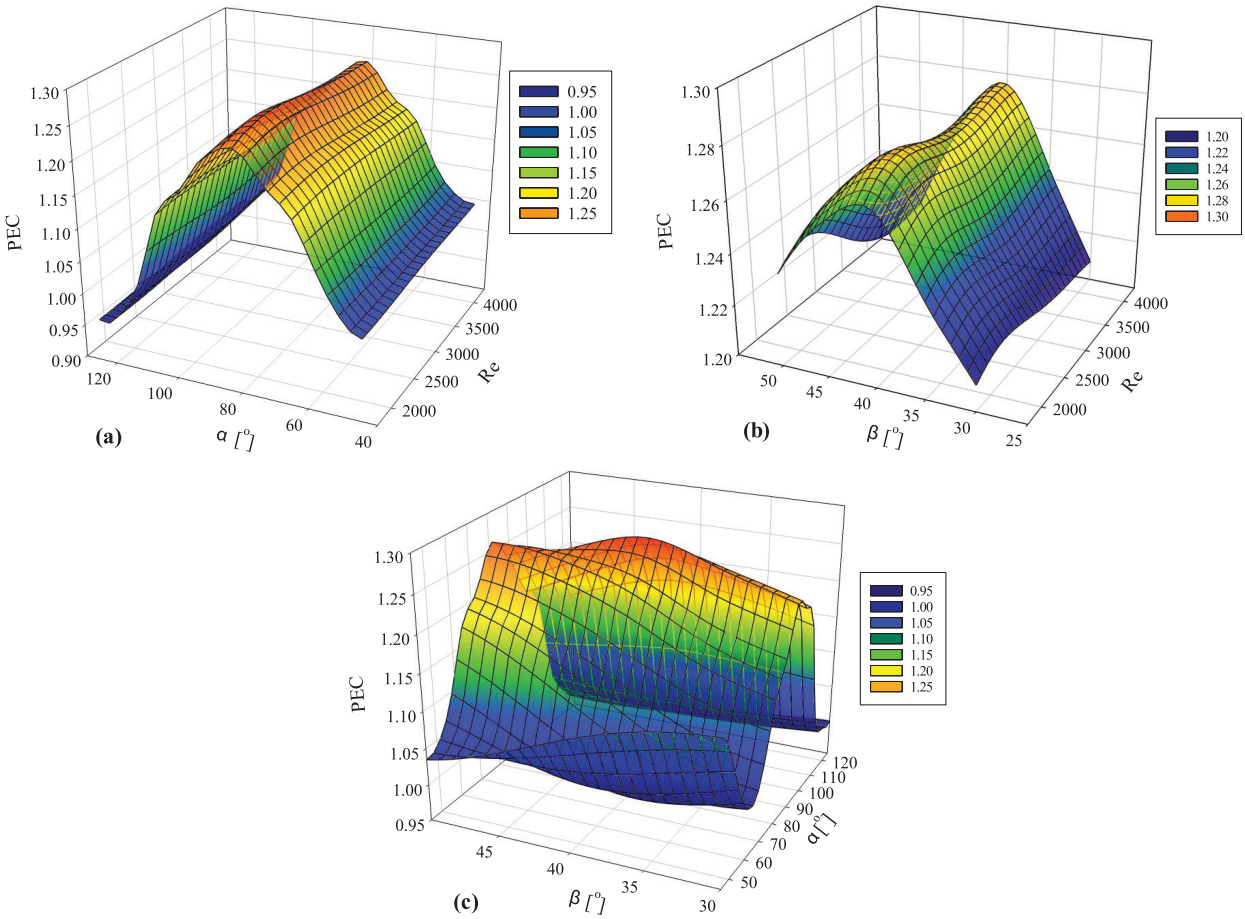

Figure 9. PEC values with the variation of (a) α -Re, (b) β-Re, and (c) α - β.

representation. A PEC value greater than 1 indicates that the system operates efficiently in terms of both heat transfer and flow resistance. In Figure 9(a), the effect of position angle and Re on PEC values is analyzed. According to Figure 9(a), it is observed that the PEC value is largely independent of the Reynolds number. However, the PEC value is highly sensitive to variations in the position angle, with moderate position angles providing the optimal operating conditions. Specifically, when the position angle is around 90-100°, up to 25% improvement in PEC values is achieved. A closer inspection of the figure reveals that changes in PEC values for the position angle are largely independent of the Re. Figure 9(b) examines the effect of arc angle and Re on PEC values. Beyond a Re of 2500, variations in PEC values are primarily influenced by changes in the arc angle. However, within the Reynolds number range of 1718 to 4296, significant improvements in PEC values are observed for moderate arc angles, with values reaching approximately 1.25. Furthermore, when the increase in surface area resulting from VGs is factored into the Nu, a thermal-hydraulic performance gain of around 40% is noted. Figure 9(c) explores the combined effect of position angle and arc angle on PEC values. The optimum *PEC* values are found at α = 90° and β = 40°. It is also noted that at low arc angles, both high and low position angles significantly reduce PEC values, indicating the importance of balancing these parameters for optimal performance. As observed in Figure 9, the variation of inputs in all three figures indicates a non-linear behavior of the PEC. This observation highlights the necessity of an effective design approach to determine the optimal values.

Overall, the findings of this study highlight the critical role of VG placement and design in optimizing heat transfer and flow characteristics in FTHEs. The results demonstrate that selecting an appropriate position angle and arc angle can significantly enhance heat transfer efficiency while maintaining an acceptable level of pressure drop. Specifically, at α = 90° and β = 40°, the PEC reached its maximum, indicating an optimal balance between heat transfer enhancement and flow resistance. The Kriging RSM confirmed the nonlinear nature of the relationship between VG positioning and performance, reinforcing the necessity of a well-structured design optimization approach. Furthermore, contour analyses revealed that improper VG placement could lead to increased wake regions and localized overheating, while an optimized configuration minimizes temperature gradients and enhances turbulence. These findings provide valuable insights for the design and

implementation of VGs in FTHE applications, emphasizing the importance of carefully balancing thermal performance and pressure drop to achieve maximum system efficiency. However, this study has certain limitations that should be acknowledged. First, the numerical simulations are based on specific assumptions, including steady-state flow and idealized boundary conditions, which may not fully capture real-world operational variations. Additionally, the analysis focuses on a limited range of Re and VG configurations, and further studies could explore a broader parameter space. Moreover, the impact of VG implementation on pressure drop and its trade-off with thermal performance should be examined in future work, particularly in the context of industrial applications. Despite these limitations, the findings provide valuable insights into the role of VG positioning and sizing in enhancing heat transfer in fin-and-tube heat exchangers.

CONCLUSION

This study emphasizes the substantial advantages of curved trapezoidal vortex generators in improving the thermal performance of fin-and-tube heat exchangers, while simultaneously underlining the possible decrease in heat transfer resulting from improper design. By conducting a comprehensive parametric analysis using the Kriging Response Surface Methodology, the optimal configurations for position angle (α) and arc angle (β) that maximize performance evaluation criteria (PEC) values have been identified according to different Reynolds numbers. The study reveals that curved trapezoidal vortex generators enhance thermal performance while keeping pressure drops within acceptable limits. Both the position angle and arc angle are key factors in optimizing heat transfer and minimizing flow resistance. The optimal configuration, with position angles between 90° and 100° and arc angles between 40° and 50°, results in up to a 27% performance improvement. Heat transfer enhancements are up to 48.5% compared to a baseline case without vortex generators, while the friction factor increased by 67%, with larger angles leading to higher increases. Generally, the curved trapezoidal vortex generator design proved to be an efficient strategy for boosting energy efficiency while minimizing flow resistance penalties. However, it is concluded that poorly positioned or improperly sized vortex generators can deteriorate thermo-hydraulic performance. These findings confirm that identifying the right combination of attack and arc angles is key to maximizing the efficiency of fin-and-tube heat exchangers. In future studies, the effects of the proposed design can be further explored by investigating staggered arrangements, different tube geometries, and heat exchangers with varying characteristic lengths under different flow conditions.

AUTHORSHIP CONTRIBUTIONS

Authors equally contributed to this work.

DATA AVAILABILITY STATEMENT

The authors confirm that the data that supports the findings of this study are available within the article. Raw data that support the finding of this study are available from the corresponding author, upon reasonable request.

CONFLICT OF INTEREST

The authors declared no potential conflicts of interest with respect to the research, authorship, and/or publication of this article.

ETHICS

There are no ethical issues with the publication of this manuscript.

REFERENCES

[1] Okbaz A, Pınarbaşı A, Olcay AB, Aksoy MH. An experimental, computational and flow visualization study on the air-side thermal and hydraulic performance of louvered fin and round tube heat exchangers. Int J Heat Mass Transf 2018;121:153–169. [CrossRef]

[2] Mohapatra T, Rout SK. Experimental investigation and performance optimization of a cross flow heat exchanger by entropy generation minimization approach. J Therm Eng 2019;5:1–12. [CrossRef]

[3] Gönül A, Okbaz AB. Enhanced performance of a microchannel with rectangular vortex generators. J Therm Eng 2023;9:260–278. [CrossRef]

[4] Gönül A, Okbaz A, Kayaci N, Dalkilic AS. Flow optimization in a microchannel with vortex generators using genetic algorithm. Appl Therm Eng 2022;201:117738. [CrossRef]

[5] Jacobi AM, Shah RK. Heat transfer surface enhancement through the use of longitudinal vortices: A review of recent progress. Exp Therm Fluid Sci 1995;11:295–309. [CrossRef]

[6] Oh Y, Kim K. Effects of position and geometry of curved vortex generators on fin-tube heat-exchanger performance characteristics. Appl Therm Eng 2021;189:116736. [CrossRef]

[7] Biswas G, Chattopadhyay H, Sinha A. Augmentation of heat transfer by creation of streamwise longitudinal vortices using vortex generators. Heat Transf Eng 2012;33:406–424. [CrossRef]

[8] Fiebig M. Vortices and heat transfer. ZAMM Zeitschrift fur Angew Math und Mech 1997;77:3–18. [CrossRef]

[9] Salviano LO, Dezan DJ, Yanagihara JI. Optimization of winglet-type vortex generator positions and angles in plate-fin compact heat exchanger: Response Surface Methodology and Direct Optimization. Int J Heat Mass Transf 2015;82:373–387. [CrossRef]

[10] da Silva FA, Dezan DJ, Pantaleão AV, Salviano LO. Longitudinal vortex generator applied to heat transfer enhancement of a flat plate solar water heater. Appl Therm Eng 2019;158:113790. [CrossRef]
[11] Md Salleh MF, Mohammed HA, Wahid MA. Thermal and hydraulic characteristics of trapezoidal winglet across fin-and-tube heat exchanger (FTHE). Appl Therm Eng 2019;149:1379–1393. [CrossRef]
[12] Leu JS, Wu YH, Jang JY. Heat transfer and fluid flow analysis in plate-fin and tube heat exchangers with a pair of block shape vortex generators. Int J Heat Mass Transf 2004;47:4327–4338. [CrossRef]
[13] Samadifar M, Toghraie D. Numerical simulation of heat transfer enhancement in a plate-fin heat exchanger using a new type of vortex generators. Appl Therm Eng 2018;133:671–681. [CrossRef]
[14] Lin CN, Liu YW, Leu JS. Heat transfer and fluid flow analysis for plate-fin and oval tube heat exchangers with vortex generators. Heat Transf Eng 2008;29:588–596. [CrossRef]
[15] Xie J, Lee HM. Flow and heat transfer performances of directly printed curved-rectangular vortex generators in a compact fin-tube heat exchanger. Appl Therm Eng 2020;180:115830. [CrossRef]
[16] Lin ZM, Liu CP, Lin M, Wang LB. Numerical study of flow and heat transfer enhancement of circular tube bank fin heat exchanger with curved delta-winglet vortex generators. Appl Therm Eng 2015;88:198–210. [CrossRef]
[17] Sharma R, Mishra DP, Wasilewski M, Brar LS. Application of response surface methodology and artificial neural network to optimize the curved trapezoidal winglet geometry for enhancing the performance of a fin-and-tube heat exchanger. Energies 2023;16:4209. [CrossRef]
[18] Sarangi SK, Mishra DP, Ramachandran H, Anand N, Masih V, Brar LS. Analysis and optimization of the curved trapezoidal winglet geometry in a high-efficiency compact heat exchanger. Int J Therm Sci 2021;164:1–15. [CrossRef]
[19] Zhou G, Ye Q. Experimental investigations of thermal and flow characteristics of curved trapezoidal winglet type vortex generators. Appl Therm Eng 2012;37:241–248. [CrossRef]
[20] Gönül A, Karayiannis TG. Pressure Drop and Heat Transfer Characteristics in a Microchannel with Pin-Fins. J Fluid Flow Heat Mass Transf 2024;11:187–196. [CrossRef]
[21] Gönül A. Enhancement of heat transfer characteristics in wavy microchannel heat sinks with streamlined micropins within convergent-divergent flow passages. Appl Therm Eng 2025;258:124574. [CrossRef]
[22] Alnakeeb MA, Saad MA, Hassab MA. Numerical investigation of thermal and hydraulic performance of fin and flat tube heat exchanger with various aspect ratios. Alexandria Eng J 2021;60:4255–4265. [CrossRef]
[23] Zhang L, et al. Numerical study of fin-and-tube heat exchanger in low-pressure environment: Air-side heat transfer and frictional performance, entropy generation analysis, and model development. Entropy 2022;27:1–9. [CrossRef]
[24] Song K, Sun K, Lu XJ, Gao QF, Hou QZ, Gu BD. Effect of wavy delta winglet vortex generators on heat transfer performance of a fin-and-tube heat exchanger. Int J Heat Fluid Flow 2024;108:109485. [CrossRef]
[25] Kim YS, Park IJ, Kim JG. Simulation approach for cathodic protection prediction of aluminum fin-tube heat exchanger using boundary element method. Metals Basel 2019;9:1–15. [CrossRef]
[26] Andreatta F, Lanzutti A, Fedrizzi L. Corrosion behaviour of AA8xxx aluminium fins in heat exchangers. Surf Interface Anal 2016;48:789–797. [CrossRef]
[27] Saini P, Shah MP. Performance evaluation of finned tube heat exchanger using curved wavy delta winglet vortex generators with circular perforations. Int Commun Heat Mass Transf 2024;159:108184. [CrossRef]
[28] ANSYS Fluent User's Guide. 15th ed. Canonsburg, PA: ANSYS Inc.; 2013.
[29] Žukauskas A, Ulinskas R. Efficiency parameters for heat transfer in tube banks. Heat Transf Eng 1985;6:19–25. [CrossRef]
[30] Gholami AA, Wahid MA, Mohammed HA. Heat transfer enhancement and pressure drop for fin-and-tube compact heat exchangers with wavy rectangular winglet-type vortex generators. Int Commun Heat Mass Transf 2014;54:132–140. [CrossRef]
[31] Ozsen M, Yildiz S. Numerical performance analysis of delta vortex generator located upstream of in-line tube bundle. Therm Sci 2024;28:2891–2903. [CrossRef]
[32] Cengel YA. Heat and Mass Transfer: Fundamentals and Applications. New York: McGraw-Hill Higher Education; 2011.
[33] Song KW, Tagawa T, Chen ZH, Zhang Q. Heat transfer characteristics of concave and convex curved vortex generators in the channel of plate heat exchanger under laminar flow. Int J Therm Sci 2019;137:215–228. [CrossRef]
[34] Gönül A, Ağra Ö. Investigation of heat transfer in tandem and staggered arrangement of wires on single layer wire-on-tube condensers in cross-flow. Int J Heat Mass Transf 2020;158:119923. [CrossRef]
[35] Box GEP, Wilson KB. On the experimental attainment of optimum conditions. J R Stat Soc Ser B 1951;13:1–38. [CrossRef]
[36] Box GEP, Behnken DW. Some new three level designs for the study of quantitative variables. Technometrics 1960;2:455–475. [CrossRef]
[37] ANSYS DesignXplorer User's Guide. Canonsburg, PA: ANSYS Inc.; 2011.